Encoderless Five-phase PMa-SynRM Drive System Based on Robust Torque-speed Estimator with Super-twisting Sliding Mode Control

Ghada A. Abdel Aziz, *Member, IEEE,* and Rehan Ali Khan

***Abstract*—In this paper, a robust torque speed estimator (RTSE) for linear parameter changing (LPC) system is proposed and designed for an encoderless five-phase permanent magnet assisted synchronous reluctance motor (5-phase PMa-SynRM). This estimator is utilized for estimating the rotor speed and the load torque as well as can solve the speed sensor fault problem, as the feedback speed information is obtained directly from the virtual sensor. In addition, this technique is able to enhance the 5-phase PMa-SynRM performance by estimating the load torque for the real time compensation. The stability analysis of the proposed estimator is performed via Schur complement along with Lyapunov analysis. Furthermore, for improving the 5-phase PMa-SynRM performance, five super-twisting sliding mode controllers (ST-SMCs) are employed with providing a robust response without the impacts of high chattering problem. A super-twisting sliding mode speed controller (ST-SMSC) is employed for controlling the PMa-SynRM rotor speed, and four super-twisting sliding mode current controllers (ST-SMCCs) are employed for controlling the 5-phase PMa-SynRM currents. The stability analysis and the experimental results indicate the effectiveness along with feasibility of the proposed RTSE and the ST-SMSC with ST-SMCCs approach for a 750-W 5-phase PMa-SynRM under load disturbance, parameters variations, single open-phase fault, and adjacent two-phase open circuit fault conditions.**

***Index Terms*—Five-phase permanent magnet assisted synchronous reluctance motor, Encoderless control, Super-twisting sliding mode control, Torque-speed estimator.**

NOMENCLATURE

V_{qp}, V_{dp}	The principal *q-d* stator voltages
I_{qp}, I_{dp}	The principal *q-d* stator currents
V_{qs}, V_{ds}	The seconder *q-d* stator voltages
I_{qs}, I_{ds}	The seconder *q-d* stator currents
L_p	The principal stator inductance
L_s	The seconder stator inductance
R_s	Stator resistance per phase
P	Number of pair-poles
ω_r	The rotor mechanical speed
ω_r^*	The speed command
θ_r	The rotor mechanical position angle
J	The rotor inertia
T_L	The external load torque
F	The damping coefficient

Manuscript received August 15, 2022; revised September 23, 2022; accepted October 08, 2022. Date of publication March 25, 2023; Date of current version January 17, 2023.

Ghada A. Abdel Aziz is with Power Electronics and Energy Conversion Department, Electronics Research Institute, Cairo, 11843, Egypt.(e-mail: ghada_ahmed@ieee.org)

Rehan Ali Khan is with Department of Electrical Engineering, University of Science & Technology, Bannu, 28100, Pakistan.

(Corresponding Author: Ghada A. Abdel Aziz)

Digital Object Identifier 10.30941/CESTEMS.2023.00020

I. INTRODUCTION

RECENTLY for accommodating the upward increasing of the consumer demand for high-power density devices, the multiphase machines have been emerged, which present substitute solutions to the conventional three-phase machines via increasing the number of motor phases. These machines have been designated for numerous applications in the electric propulsion, electric vehicles, along with aerospace [1]–[3]. One of these multiphase machines, is the five-phase permanent magnet assisted synchronous reluctance motors (5-phase PMa-SynRMs). These machines have the inherent characteristics of high torque–inertia ratio, rapid control response, high power factor, high efficiency, fault-tolerant aptitude due to the greater number of phases available along with high-power density [4].

It is well known that rotor position information is significantly needed for motor precision control and this information need to be continuously known for synchronizing the stator currents with the PMa-SynRM rotor permanent magnet flux, which alters with rotor rotation [5]. This information is attained via utilizing position sensor e.g. resolver, optical encoder, and etc. Nevertheless, these position sensors not only increase complexity, cost, along with maintenance, but also degrade the drive system reliability and robustness. Consequently, great efforts have been performed in developing sensorless control approaches for the five-phase permanent magnet machines.

In [6], a sliding mode control combined with an extended Kalman filter estimator have been employed for estimating the rotor speed of a 5-phase permanent magnet synchronous machine. Kalman filter has been used for obtaining high precision estimations along with processing the noisy measurements. Via employing both the extended Kalman filter estimator for estimating the rotor speed and the sliding mode speed controller, a good control respoinse has been obtained with low cost and high reliability. However, the proposed estimator and the sliding mode controller were not

investigated experimentally.

In [7], an encoderless backstepping drive has been introduced for a 5-phase PMSM through utilizing an indefinite input estimator for estimating the rotor speed and the load torque. The backstepping control has solved the speed sensor fault problem, as the feedback speed information has been presumed from the virtual sensor. The indefinite input estimator and the backstepping controller gains have been carefully chosen for improving the estimation accuracy and stability dynamic performance.

In [8], an adaptive linear neural network has been introduced for estimating the rotor position of a 5-phase PMSM with a high accuracy during the low speed operation without high frequency signal injection. Although, a better response of the Adaline was attained compared to the phase locked loop throughout the starting from indefinite states, the torque response has high torque ripples.

In [9], a brand new encoderless field-oriented control has been introduced for a 5-phase PMSM via exploiting the freewheeling current for accommodating both position sensor and IGBT failures that is anticipated to improve the drive's fault-tolerant aptitude. Although, the proposed encoderless control was less parameterized, it suffers from the poor compatibility with a generic 5-phase PMSM characterized through the time-variant mutual- and self inductances.

As the existence of indefinite, time changing, and load-torque inputs, unknowing the initial rotor's position angle, and the indefinite motor parameters can degrade the drive system performance, thus, various researches have been developed for coping with this problem. In [10], a high-gain generalized proportional integral (PI) estimator-based active disturbance rejection controller has been developed for the PMSM. This controller has been designed on the basis of the direct measurability of the system's outputs, constituted through the PMSM's *d*-axis current and the angular displacement. In [11], an extended state estimator has been designed for estimating the PMSM's total disturbance and feedforward compensation has been employed for suppressing the system disturbance. Although, the proposed estimator has suppressed the indefinite system disturbance, its structure is very complex and has high computational time. In [12], an anti-disorder output feedback dynamic surface control approach has been introduced for tracking the interior PMSM position that was subjected to time-varying disturbances and indefinite nonlinearities. In addition, a nonlinear extended-state-estimator has been designed based on exponential functions for estimating the external disturbances and system uncertainties. Although, this estimator estimated preciously the system uncertainties, a position measurement is required for attaining the expected anti-disorder response.

This paper aims to design a robust torque-speed estimator (RTSE) for estimating the rotor speed and the load torque for a five-phase permanent magnet assisted synchronous reluctance motor (5-phase PMa-SynRM). Thus, no speed sensor is needed for measuring the rotor speed and therefore, the drive system cost is low. Moreover, this estimator can solve the speed sensor fault problem, as the feedback speed information is acquired directly from the virtual sensor. Furthermore, for enhancing the dynamic performance of the 5-phase PMa-SynRM, five super-twisting sliding mode controllers are employed for controlling the rotor speed and the PMa-SynRM currents. Fig. 1 illustrates the block diagram of the encoderless 5-phase PMa-SynRM drive system with the RTSE, super-twisting sliding mode current controllers (ST-SMCCs) for the *dq*-axis currents, and the super-twisting sliding mode speed controller (ST-SMSC) using the space vector pulse width modulation. The detailed design structure of the whole drive system is introduced in this paper.

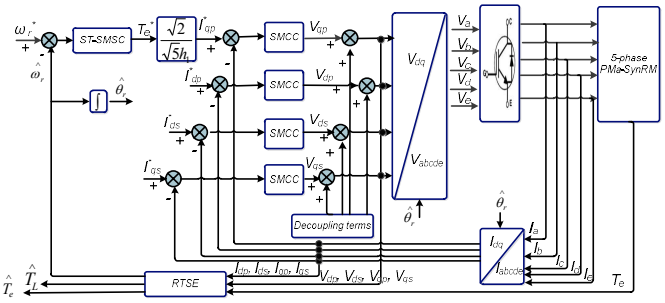

Fig. 1. The encoderless 5-phase PMa-SynRM drive system with the RTSE, ST-SMCCs, and the ST-SMSC.

The paper structure is prepared as follows: the mathematical representation of the 5-phase PMa-SynRM is derived in Section II. Section III presents the detailed design of the RTSE estimator for the 5-phase PMa-SynRM. The stability analysis of the proposed estimator is presented in Section IV. Section V introduces the stages for computing the proposed estimator for the 5-phase PMa-SynRM. Section VI presents the detailed design of the super-twisting sliding mode speed and the four currents controllers for the 5-phase PMa-SynRM. The experimental verification of the proposed encoderless 5-phase PMa-SynRM with the RTSE, ST-SMSC, and the ST-SMCCs is introduced in Section VII and Section VIII finally draws the conclusion of this paper.

II. THE 5-PHASE PMA-SYNRM MATHEMATICAL REPRESENTATION

The dynamic representation of the 5-phase PMa-SynRM in the *dq*-frame is represented by:

$$V_{dp} = R_s I_{dp} - P\omega_r L_p I_{qp} + L_p \frac{dI_{dp}}{dt} \quad (1)$$

$$V_{qp} = R_s I_{qp} + P\omega_r L_p I_{dp} + L_p \frac{dI_{qp}}{dt} + \sqrt{\frac{5}{2}} h_1 \omega_r \quad (2)$$

$$V_{ds} = R_s I_{ds} - 3P\omega_r L_s I_{qs} + L_s \frac{dI_{ds}}{dt} \quad (3)$$

$$V_{qs} = R_s I_{qs} + P\omega_r L_s I_{ds} + L_s \frac{dI_{qs}}{dt} - \sqrt{\frac{5}{2}} h_3 \omega_r \quad (4)$$

where h_1 & h_3 denote the 1st & 3rd harmonic constants, respectively. The mechanical representation of the 5-phase PMa-SynRM in the *dq*-frame can be expressed as:

$$J\frac{d\omega_r}{dt} = T_e - F\omega_r - T_L \quad (5)$$

$$T_e = \sqrt{\frac{5}{2}}\left(h_1 I_{qp} - h_3 I_{qs}\right) \quad (6)$$

III. The Torque-Speed Estimator for Linear Parameter Changing System

For approximating a real nonlinear system, thus, the linear parameter changing can be utilized for representing this system. Through this representation, a simple linear model for nonlinear systems can be designed with matrices contingent on algebraic constraints as well as can be employed in various applications. In this paper, the LPC system is utilized for simplifying the 5-phase PMa-SynRM model in the *dq*-frame.

A. System Depiction Equations

The LPC representation of the 5-phase PMa-SynRM in the state space forms of (1)-(6) with considering the indefinite input can be expressed by (7) & (8):

$$\frac{dX}{dt} = M\left(I_{dp}, I_{ds}\right)X(t) + WU(t) + DT(t) \quad (7)$$

$$Y(t) = NX(t) \quad (8)$$

where

$M\left(I_{dp}, I_{ds}\right) = \begin{bmatrix} M_{11} & M_{12} \\ M_{21} & M_{22} \end{bmatrix}$, $N = \begin{bmatrix} 1 & 0 \end{bmatrix}$, $D = \begin{bmatrix} 0 \\ -1/J \end{bmatrix}$,

$W = \sqrt{\frac{5}{2}}\begin{bmatrix} h_1/L_p & -h_3/L_s & -h_1R_s/L_p & h_3R_s/L_s \\ 0 & 0 & 0 & 0 \end{bmatrix}$

$M_{11}=0$, $M_{21}=1/J$, $M_{22}=-F/J$,

$M_{12} = \sqrt{\frac{5}{2}}P\left(3h_3 I_{ds} - h_1 I_{dp}\right) - \frac{5}{2}\left(\frac{h_1^2}{L_p} + \frac{h_3^2}{L_s}\right)$

The state vector can be represented by $X(t) = \begin{bmatrix} T_e & \omega_r \end{bmatrix}^T \in \Re^{\mu}$, meanwhile, the control input vector can be expressed by $U(t) = \begin{bmatrix} V_{qp} & V_{qs} & I_{qp} & I_{qs} \end{bmatrix}^T \in \Re^{r}$, and the indefinite input vector can be expressed by $T(t) = \begin{bmatrix} T_L \end{bmatrix} \in \Re^{Q}$. Both the I_{ds} & I_{dp} are the bounded time-changing parameters and supposed to be identified. In addition, $I_{ds\_min} \le I_{ds} \le I_{ds\_max}$ & $I_{dP\_min} \le I_{dP} \le I_{dP\_max}$.

Afterwards, the matrix *M* can be deduced that it is bounded and can be expressed by the following form:

$$M = M\left(I_{dp}, I_{ds}\right) = \sum_h \xi^h\left(I_{dp}, I_{ds}\right)M_h \quad (9)$$

where $0 \le \xi^h\left(I_{dp}, I_{ds}\right) \le 1$ & $\sum_h \xi^h\left(I_{dp}, I_{ds}\right) = 1$

W, N & D are considered constant matrices with proper dimensions. Typically, the aforementioned system can be expressed by the polytopic representation as in (10) & (11):

$$\frac{dX}{dt} = \sum_h \xi^h\left(I_{dp}, I_{ds}\right)M_h X(t) + WU(t) + DT(t) \quad (10)$$

$$Y(t) = NX(t) \quad (11)$$

The presence of a full-order indefinite input estimator necessitates two conditions to be verified [7], [13]-[14]. The relative condition is *rank (ND)= rank (D)=Q* that forces this (12) as follows:

$$dim(m) \le dim(Y) \quad (12)$$

The minimal phase condition is similar to the Hautus criteria for observability:

$$rank\begin{bmatrix} I_{\mu} - M & -D \\ N & 0 \end{bmatrix} = \mu + Q \quad (13)$$

If (13) is not fulfilled, thus, the augmented system can be employed as the observability conditions are less obstructive. The augmented system in the updated state space form is represented by:

$$B\frac{dX_{aug}}{dt} = M_{aug}\left(I_{dp}, I_{ds}\right)X_{aug}(t) + W_{aug}U_{aug}(t) \quad (14)$$

$$Y_{aug}(t) = N_{aug}X_{aug}(t) \quad (15)$$

where $B = \begin{bmatrix} I_{\mu} & 0 \\ 0 & 0 \end{bmatrix}$, $M_{aug} = \begin{bmatrix} M & 0 \\ 0 & -\beta \end{bmatrix}$, $W_{aug} = \begin{bmatrix} W & 0 \\ 0 & \varphi \end{bmatrix}$,

$N_{aug} = \begin{bmatrix} N & 0 \end{bmatrix}$, $X_{aug} = \begin{bmatrix} X \\ m \end{bmatrix}$, $U_{aug} = \begin{bmatrix} U \\ m \end{bmatrix}$, $Y_{aug} = \begin{bmatrix} Y \\ m \end{bmatrix}$.

The linear augmented system is observable when:

$$rank\begin{bmatrix} B & M_{aug} \\ 0 & N_{aug} \\ 0 & B \end{bmatrix} = \mu + rankB \quad (16)$$

Afterwards:

$$rank\begin{bmatrix} B \\ B^{\perp}M_{aug} \\ N_{aug} \end{bmatrix} = \mu \quad (17)$$

where $B^{\perp}$ denotes the *B* orthogonal matrix with a full row rank matrix as $B^{\perp}B = 0$.

B. The Robust Torque-Speed Estimator Design

Once the conditions of (16) & (17) are fulfilled, the RTSE representation can be expressed by[15]-[16]:

$$\frac{dC(t)}{dt} = H\left(I_{dp}, I_{ds}\right)C_{aug}(t) + \alpha U_{aug}(t) + \gamma Y_{aug}(t) \quad (18)$$

$$\hat{X}_{aug}(t) = C(t) - qB^{\perp}W_{aug}U_{aug}(t) + GY_{aug}(t) \quad (19)$$

where $\hat{X}_{aug}(t)$ denotes the estimated state vector of $X_{aug}(t)$ meanwhile, *C* denotes the estimator state vector.

The $H(I_{dp}, I_{ds})$ matrix can be expressed by (20):

$$H\left(I_{dp}, I_{ds}\right) = \sum_{h=1}^{h=H} \xi^h\left(I_{dp}, I_{ds}\right)H_h \quad (20)$$

According to (20), the matrix *H* can be bounded via H_{max} & H_{min}. The Matrices *H, α, γ, A, q & G* are indefinite with proper dimensions and changing parameters with time.

These matrices must be distinct with the state error $E(t) = \hat{X}_{aug}(t) - X_{aug}(t)$ & the error between *C(t)* & $TBX_{aug}(t)$, noted $e(t) = C(t) - TBX_{aug}(t)$ approximately zero.

The convergence conditions of the RTSE can be expressed by[17]:

$$\begin{cases} HTB + \gamma N_{aug} - TM_{aug} = 0 \\ \alpha - TW_{aug} = 0 \\ ATB + qB^{\perp}M_{aug} + GN_{aug} = I_{\mu} \end{cases} \quad (21)$$

Afterwards, the *e(t)* dynamic and *E(t)*, which denotes the state estimation error can be represented by (22) & (23):

$$\frac{de(t)}{dt} = He(t) \quad (22)$$

$$E(t) = Ae(t) \quad (23)$$

The main challenge of designing the RTSE is to find the matrices *H, α, γ, A, q, T & G* provided both (22) & (23) are fulfilled for making the the errors *E(t)* & *e(t)* converge to zero.

IV. The Stability Analysis

Lyapunov candidates' functions can be chosen as:

$$V_1 = V_1\left(I_{dp}, I_{ds}\right) = e^T Z_1\left(I_{dp}, I_{ds}\right)e = e^T Z_1 e \succ 0 \quad (24)$$

$$V_2 = V_2\left(I_{dp}, I_{ds}\right) = E^T Z_2\left(I_{dp}, I_{ds}\right)E = E^T Z_2 E \succ 0 \quad (25)$$

where Z_1 & Z_2 are symmetrical and positive definite matrices.

Via the derivative of V_1 & V_2, one gets:

$$\begin{aligned}\frac{dV_1}{dt} &= \frac{de^T}{dt}Z_1 e + e^T Z_1 \frac{de}{dt} \\ &= e^T\left(\left(Z_1 H\right)^T + \left(Z_1 H\right)\right)e \prec 0\end{aligned} \quad (26)$$

$$\begin{aligned}\frac{dV_2}{dt} &= \frac{dE^T}{dt}Z_2 E + E^T Z_2 \frac{dE}{dt} \\ &= E^T\left(\left(Z_2 AH\right)^T A + A^T Z_2 AH\right)E \prec 0\end{aligned} \quad (27)$$

The disparity $dV_1(t)/dt < 0$ & $dV_2(t)/dt < 0$ are valid for all $e(t) \neq 0$ & $E(t) \neq 0$ if and only if:

$$\left(Z_1 H\right)^T + \left(Z_1 H\right) \prec 0 \ \ \& \ \ \left(Z_2 AH\right)^T A + A^T Z_2 AH \prec 0$$

V. Stages for Computing RTSE for LPC System

Through this section, the detailed stages for computing and obtaining the solution of the RTSE for the linear parameter changing system are presented as follows:

Stage # 1: Establishing the Sylvester equations:

Considering the Sylvester equations (21), and supposing that $T = T + \tau B^{\perp}$ where τ denotes an arbitrary matrix with proper dimension, thus, (21) can rewritten by:

$$\begin{bmatrix} H & \tau & \gamma \\ A & q & G \end{bmatrix}\begin{bmatrix} \overline{T}B \\ B^{\perp}M_{aug} \\ N_{aug} \end{bmatrix} = \begin{bmatrix} \overline{T}M_{aug} \\ I_{\mu} \end{bmatrix} \quad (28)$$

The (28) has a solution in case:

$$rank\begin{bmatrix} \overline{T}B \\ B^{\perp}M_{aug} \\ N_{aug} \\ \overline{T}M_{aug} \\ I_{\mu} \end{bmatrix} = rank\begin{bmatrix} \overline{T}B \\ B^{\perp}M_{aug} \\ N_{aug} \end{bmatrix} = \mu \quad (29)$$

Global solution of (28) can be expressed as:

$$\begin{bmatrix} H & \tau & \gamma \\ A & q & G \end{bmatrix}\begin{bmatrix} \overline{T}M_{aug} \\ I_{\mu} \end{bmatrix} - \delta^{+} - \begin{bmatrix} Y_1 \\ Y_2 \end{bmatrix}\left(I - \delta\delta^{+}\right) \quad (30)$$

where $\delta = \begin{bmatrix} \overline{T}B \\ B^{\perp}M_{aug} \\ N_{aug} \end{bmatrix}$ & $\begin{bmatrix} Y_1 \\ Y_2 \end{bmatrix}$ denotes an arbitrary matrix of proper dimension.

Stage # 2: The intermediate matrices construction

The subsequent matrices can be distinct through this stage as follows:

$$\Delta_A = \delta^{+}\begin{bmatrix} I \\ 0 \\ 0 \end{bmatrix},\ \Delta_q = \delta^{+}\begin{bmatrix} 0 \\ I \\ 0 \end{bmatrix},\ \Delta_G = \delta^{+}\begin{bmatrix} 0 \\ 0 \\ I \end{bmatrix},$$

$$\Delta_H = \left(I - \delta\delta^{+}\right)\begin{bmatrix} I \\ 0 \\ 0 \end{bmatrix},\ \Delta_{\tau} = \left(I - \delta\delta^{+}\right)\begin{bmatrix} 0 \\ I \\ 0 \end{bmatrix},$$

$$\Delta_{\gamma} = \left(I - \delta\delta^{+}\right)\begin{bmatrix} 0 \\ 0 \\ I \end{bmatrix},\ \begin{matrix} \Theta_H = \overline{T}M_{aug}\Delta_A \\ \Theta_{\gamma} = \overline{T}M_{aug}\Delta_G \\ \Theta_{\tau} = \overline{T}M_{aug}\Delta_q \end{matrix}$$

Based on the above equations' depiction, Θ_H, Θ_{γ}, & Θ_{τ} can be represented in polytopic form as they rely on the M_{aug} variable matrix. According to these matrices, the matrices of the estimator can be defined as:

$$\begin{matrix} H = \Theta_H - Y_1\Delta_H & A = \Delta_A - Y_2\Delta_H \\ \gamma = \Theta_{\gamma} - Y_1\Delta_{\gamma} & G = \Delta_G - Y_2\Delta_{\gamma} \\ \tau = \Theta_{\tau} - Y_1\Delta_{\tau} & q = \Delta_q - Y_2\Delta_{\tau} \end{matrix} \quad (31)$$

Stage # 3: Calculating the Y_1 & Y_2 matrices along with the RTSE matrices

The Y_1 & Y_2 matrices can be defined randomly; nevertheless, they can be obtained from the stability analysis of Lyapunov for more accuracy.

Once the Y_1 & Y_2 matrices are obtained, the (31) can be rewritten with substituting the values of Y_1 & Y_2 matrices to compute the RTSE parameters. The values of *H, A, P, q & G* are obtained from (31).

$$T = T + \tau B^{\perp} \text{ afterwards } \alpha = TW_{aug}$$

VI. The Design of the Super-twisting Sliding Mode Controllers

In this paper, five ST-SMCs are utilized. The super-twisting sliding mode speed controller (ST-SMSC) is employed for controlling the 5-phase PMa-SynRM's rotor speed and the other four super-twisting sliding mode current controllers (ST-SMCCs) are employed for controlling the four currents I_{dp}, I_{qp}, I_{ds} & I_{qs}.

A. The ST-SMSC Design for the PMa-SynRM Speed

Fig. 2 depicts the structure of the ST-SMSC, which produces the reference electromagnetic torque T_e^*. For the speed control loop, the switching function of the rotor speed $s_{\omega r}$, which denotes the difference between the ω_r^* and the estimated rotor speed $\hat{\omega}_r$ can be expressed by (32):

$$s_{\omega r} = \omega_r^* - \hat{\omega}_r \quad (32)$$

The ST-SMSC can be represented by (33) & (34):

$$T_e^* = K_{P\omega r}\left|s_{\omega r}\right|^r sgn\left(s_{\omega r}\right) + T_{e1}^* \quad (33)$$

$$\frac{dT_{e1}^*}{dt} = K_{I\omega r}\, sgn\left(s_{\omega r}\right) \quad (34)$$

where *r* represents the exponent, which can be distinct for ST-SMSC. Meanwhile, $K_{I\omega r}$ & $K_{PI\omega r}$ designate the ST-SMSC integral and proportional gains, respectively. The dynamics and response of the ST-SMSC can be adjusted via varying the exponent *r* along with ST-SMSC proportional & integral gains.

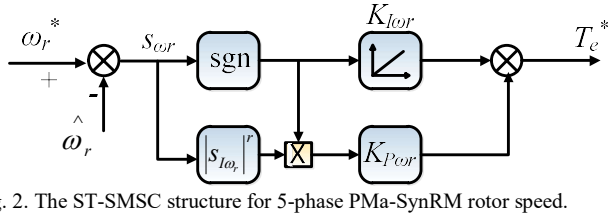

Fig. 2. The ST-SMSC structure for 5-phase PMa-SynRM rotor speed.

B. The ST-SMCCs Design for the PMa-SynRM Currents

For controlling the 5-phase PMa-SynRM currents, thus, four ST-SMCCs are employed. Fig. 3 depicts the general form of the ST-SMCC for obtaining the reference V_{dq}^*. The I_{dp} ST-SMCC controller is utilized for producing the V_{dp}. Meanwhile, I_{ds} ST-SMCC controller is utilized for producing the V_{ds}. The I_{qp} ST-SMCC controller is utilized for producing the V_{qp}. Meanwhile, I_{qs} ST-SMCC controller is utilized for producing the V_{qs}.

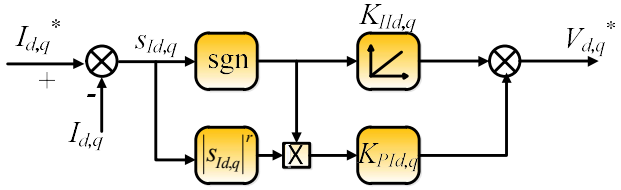

Fig. 3. The general structure of the ST-SMCC for the *dq*-axis currents.

For the principal *d-q* axis currents, the switching function $s_{Idp,qp}$, which represents the difference between the $I^*_{dp,qp}$ and $I_{dp,qp}$ can be expressed by (35):

$$s_{Idp,qp} = I^*_{dp,qp} - I_{dp,qp} \tag{35}$$

where $s_{Idp,qp}$ represents the switching function of the principal *d-q* axis currents. This controller can be represented by (36) & (37):

$$V^*_{dp,qp} = K_{PIdp,qp} \left|s_{Idp,qp}\right|^r sgn\left(s_{Idp,qp}\right) + V^*_{dp_1,qp_1} \tag{36}$$

$$\frac{dV^*_{dp_1,qp_1}}{dt} = K_{IIdp,qp}\, sgn\left(s_{Idp,qp}\right) \tag{37}$$

where $K_{IIdp,qp}$ & $K_{PIdp,qp}$ designate the principal *d-q* axis ST-SMCCs integral and proportional gains, respectively. Meanwhile, for the seconder *d-q* axis ST-SMCCs, the switching function $s_{Ids,qs}$, which represents the difference between the $I^*_{ds,qs}$ and $I_{ds,qs}$ can be expressed by (38):

$$s_{Ids,qs} = I^*_{ds,qs} - I_{ds,qs} \tag{38}$$

where $s_{Ids,qs}$ represents the switching function of the seconder *d-q* axis currents. This controller can be represented by (39) & (40):

$$V^*_{ds,qs} = K_{PIds,qs} \left|s_{Ids,qs}\right|^r sgn\left(s_{Ids,qs}\right) + V^*_{ds_1,qs_1} \tag{39}$$

$$\frac{dV^*_{ds1,qs1}}{dt} = K_{IIds,qs}\, sgn\left(s_{Ids,qs}\right) \tag{40}$$

where $K_{IIds,qs}$ & $K_{PIds,qs}$ designate the seconder *d-q* axis ST-SMCCs integral and proportional gains, respectively.

VII. Experimental Results

A. System Parameters Identifications for Experimental Work

By substituting the PMa-SynRM parameters (Table I) into (7) & (8), one gets:

$$M = \begin{bmatrix} 0 & \left(17.85I_{ds} - 6.32I_{dp}\right) - 1614.3 \\ 5494.5 & -109.89 \end{bmatrix},$$

$$D = \begin{bmatrix} 0 \\ -5494.5 \end{bmatrix} \qquad W = \begin{bmatrix} 2.47 & -4.8 & -11.87 & 22.5 \\ 0 & 0 & 0 & 0 \end{bmatrix},$$

$$N = \begin{bmatrix} 1 & 0 \end{bmatrix}$$

The comparative condition through this case is not fulfilled as *rank (ND) ≠ rank (D) = Q*, afterwards, the system is not observable. So, the augmented system represented via (14) & (15) can be used as:

TABLE I
THE 5-PHASE PMA-SYNRM SPECS

Nominal power (W)	750	Number of pair-poles	2
Nominal voltage (V)	220	Inertia of the motor & load (kg. m^2)	0.000182
Nominal speed (rpm)	3000	Friction coefficient (N.m/rad/sec)	0.02
Nominal current (A)	3	Nominal torque (N.m)	2.39
Stator resistance (Ω/phase)	2.88	PM flux (wb)	0.4366
d-axis inductance (mH/phase)	6.4	*q*-axis inductance (mH/phase)	14.6

$$N_{aug} = \begin{bmatrix} 1 & 0 & 0 \end{bmatrix}, \quad B = \begin{bmatrix} 1 & 0 & 0 \\ 0 & 1 & 0 \\ 0 & 0 & 0 \end{bmatrix}, \quad B^{\perp} = \begin{bmatrix} 0 & 0 & 0 \\ 0 & 0 & 0 \\ 0 & 0 & 1 \end{bmatrix},$$

$$M_{aug} = \begin{bmatrix} 0 & \left(17.85I_{ds} - 6.32I_{dp}\right) - 1614.3 & 0 \\ 5494.5 & -109.89 & -5494.5 \\ 0 & 0 & -\beta \end{bmatrix},$$

$$W_{aug} = \begin{bmatrix} 2.64 & -4.6 & -11.52 & 22.5 & 0 \\ 0 & 0 & 0 & 0 & 0 \\ 0 & 0 & 0 & 0 & \beta \end{bmatrix} \text{ with } I_{ds} \in [0, 0.5] \&$$

$I_{dp} \in [0, 0.5]$ through the steady-state. β denotes an arbitrary constant and M_{aug} denotes a bounded matrix. Based on this augmented system, the entire observability conditions of (16) & (17) are fulfilled. As there are two altering parameters with time, thus, there will be four linear systems for computing.

The four matrices M_{1-aug}, M_{2-aug}, M_{3-aug} & M_{4-aug} can be defined for the 4 systems, with the rest of the matrices B, W_{aug} & N_{aug} are constants. The following functions can be defined as:

$$\xi^1\left(I_{dP}\right) = \left(0.5 - I_{dP}\right)/0.5, \xi^2\left(I_{dP}\right) = 2I_{dP}$$

$$\xi^1\left(I_{ds}\right) = \left(0.5 - I_{ds}\right)/0.5, \xi^2\left(I_{ds}\right) = 2I_{ds}$$

For β=1 & $\tau = \begin{bmatrix} 1 & 0 & 0 \\ 0 & 1 & 0 \\ 0 & 0 & 1 \end{bmatrix}$, thus, $\overline{T}$ & δ can be calculated.

After resolution of the linear matrix inequality, both the matrices Y_1 & Y_2 can be employed for calculating the estimator matrices defined by (18) & (19). So, the four matrices H_1, H_2, H_3 & H_4 for the estimator can be defined as:

$$H_1 = \begin{bmatrix} -11.3 & -0.55 & 0 \\ 522.2 & -0.5 & 0 \\ 0 & 0 & -11.3 \end{bmatrix}, H_2 = \begin{bmatrix} -11.3 & -0.75 & 0 \\ 522.2 & -0.5 & 0 \\ 0 & 0 & -11.3 \end{bmatrix}$$

$$H_3 = \begin{bmatrix} -11.3 & -0.5 & 0 \\ 522.2 & -0.5 & 0 \\ 0 & 0 & -11.3 \end{bmatrix}, H_4 = \begin{bmatrix} -11.3 & -0.75 & 0 \\ 522.2 & -0.5 & 0 \\ 0 & 0 & -11.3 \end{bmatrix}$$

The rest matrices of estimators can be expressed by:

$$\alpha = \begin{bmatrix} 1.2 & -2.3 & -6.4 & 11.7 & 0 \\ 0 & 0 & 0 & 0 & -1222 \\ 0 & 0 & 0 & 0 & 0 \end{bmatrix}, A = \begin{bmatrix} 0.3 & 0 & 0 \\ 0 & 1 & 0 \\ 0 & 0 & 0 \end{bmatrix}$$

$$q = \begin{bmatrix} 0 & 0 & 0 \\ 0 & 0 & 0 \\ 0 & 0 & -1 \end{bmatrix}, G = \begin{bmatrix} 0.667 \\ 0 \\ 0 \end{bmatrix}, \gamma = \begin{bmatrix} 5.6 \\ 1055 \\ 0 \end{bmatrix}$$

B. Lab Setup

Fig. 4 depicts the lab setup for validating the proposed RTSE, AT-SMSC, and the ST-SMCCs for the encoderless 5-

phase PMa-SynRM (Table I) via utilizing dSPACE 1104. For investigating the effectiveness of the proposed encoderless approach, an optical encoder is mounted on the 5-phase PMa-SynRM shaft. The pulse width modulation converter is employed for driving the system. Both 10 & 1 kHz sampling frequencies are chosen for the current and speed loops, respectively. The effectiveness of the proposed RTSE, ST-SMSC, and the ST-SMCCs for the 5-phase PMa-SynRM are investigated experimentally through these cases.

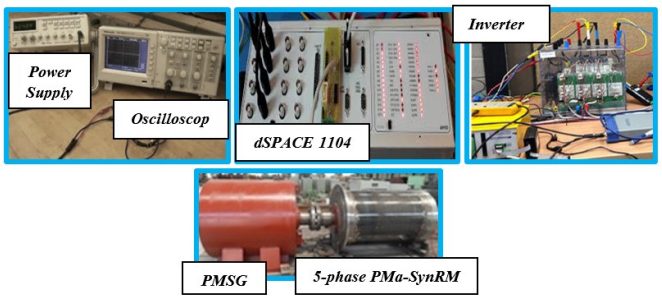

Fig. 4. The hardware platform for the 5-phase PMa-SynRM drive system.

C. Sensitivity to Speed Commands and Load Torque Disturbances

Fig. 5 depicts the 5-phase PMa-SynRM performance using the RTSE, ST-SMSC, and ST-SMCCs under different speed commands and load torque disturbances. The 5-phase PMa-SynRM starts at 25% of its rated speed from t=0−4 sec, subsequently, the speed command approaches 50% of the rated rotor speed from t=4−8 sec, afterwards, it reaches the full rated speed throughout t=8−10 sec. In addition, a load torque disturbance is occurred with full load at t=2 sec then, it is 50% of the rated torque at t=6 sec. Based on Fig. 5, there is a superior tracking performance between the estimated rotor speed (Est. speed) of the 5-phase PMa-SynRM along with the measured speed (Meas. Speed) via the speed sensor. Moreover, there is a superior tracking between the T_L^* and the estimated T_L and the T_e and the estimated T_e. In addition, there is a superior tracking between the T_e and the estimated T_e. Furthermore, for the torque response, the torque ripples at the no-load condition are 7%, meanwhile, for the half-load

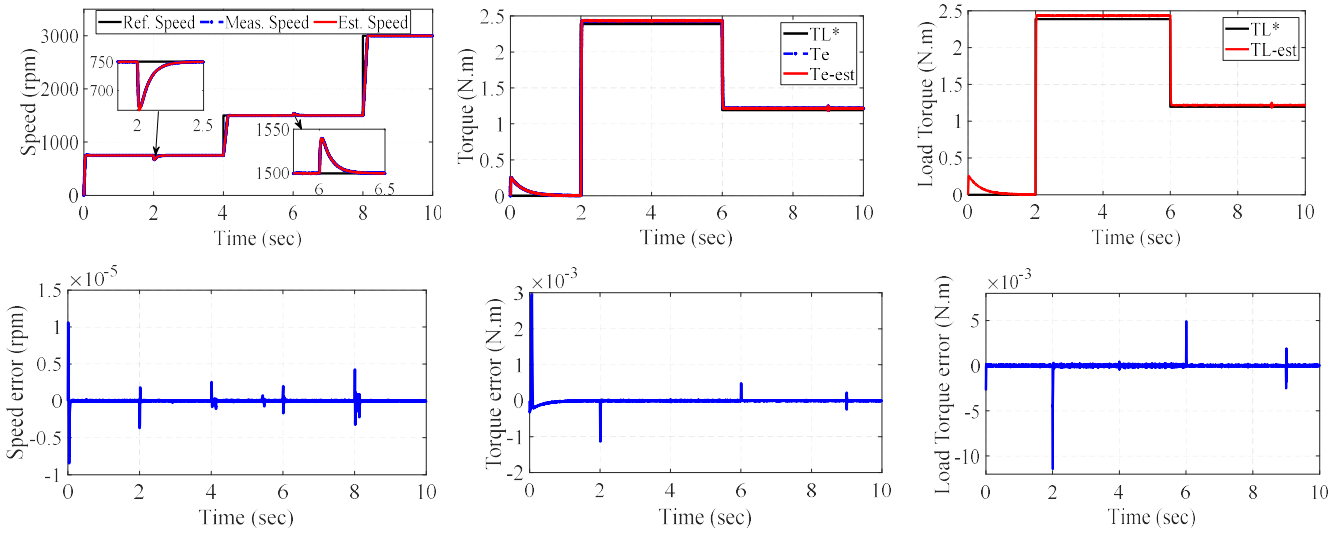

Fig. 5. The 5-phase PMa-SynRM performance using the proposed RTSE, ST-SMSC, and ST-SMCCs at different speed command and load torque disturbances.

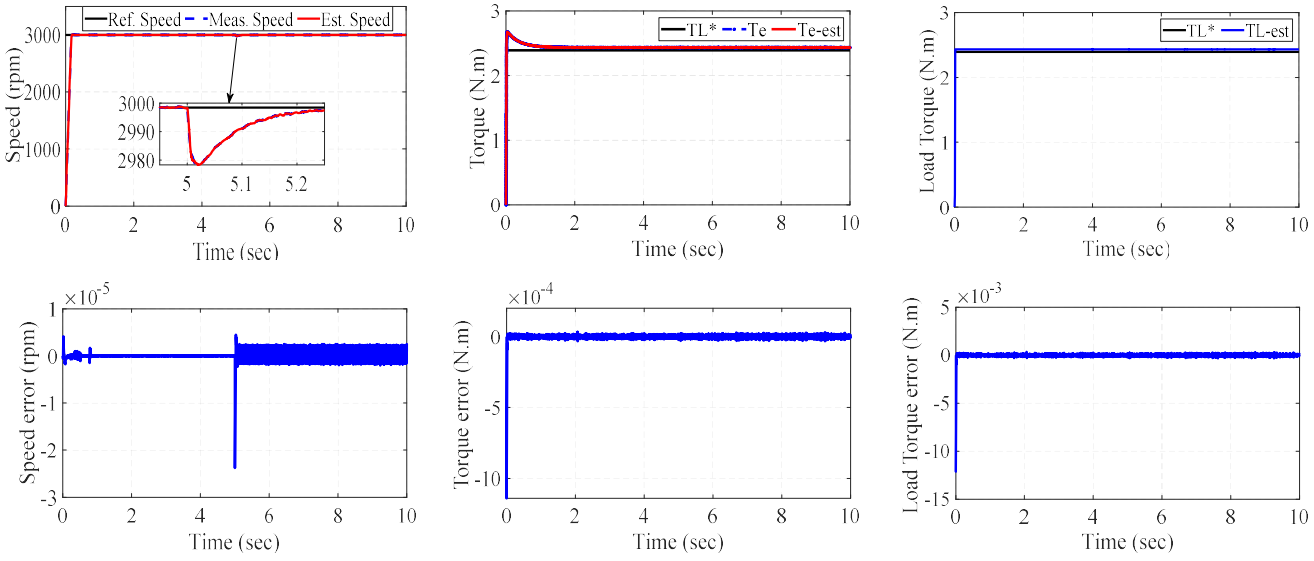

Fig. 6. The 5-phase PMa-SynRM performance using the proposed RTSE, ST-SMSC, and ST-SMCCs at stator resistance and L_q variation condition.

condition, the torque ripples are 8%, and for the full load condition, the torque ripples are 9%. This superior tracking between the actual signals and the estimated signals and low torque ripples prove the effectiveness of the proposed RTSE for estimating the rotor speed and the load torque plus the well-designed ST-SMSC.

D. Sensitivity to Stator Resistance and Lq Variation Condition

Fig. 6 depicts the 5-phase PMa-SynRM performance using the RTSE, ST-SMSC, and ST-SMCCs at +50% increase in stator resistance along with +50% increase in L_q at t=5 sec. As depicted, the proposed RTSE with the ST-SMSC, and ST-SMCCs proved their robustness alongside the 5-phase PMa-SynRM electrical parameter variation in the stator resistance and the L_q. In addition, the torque ripples for the torque response is 1.9%.

E. Sensitivity to the Moment of Inertia Changing Condition

Fig. 7 depicts the 5-phase PMa-SynRM performance using the RTSE, ST-SMSC, and ST-SMCCs at +50% increase in moment of inertia at t=5 sec. As depicted, the proposed RTSE with the ST-SMSC, and ST-SMCCs proved their robustness alongside the moment of inertia variation condition. In addition, the torque ripples for the torque response is 1.8%.

F. Sensitivity to the Open Fault of Phase A Condition

As the 5-phase PMa-SynRM is a multi-phase machine and it is a fault tolerant machine and in order to check the robustness of the proposed the RTSE, ST-SMSC, and ST-SMCCs performance, an open-phase fault is occurred in phase A of the 5-phase PMa-SynRM at t=5 sec and the fault tolerant control (FTC) is adopted at t=5.5 sec.

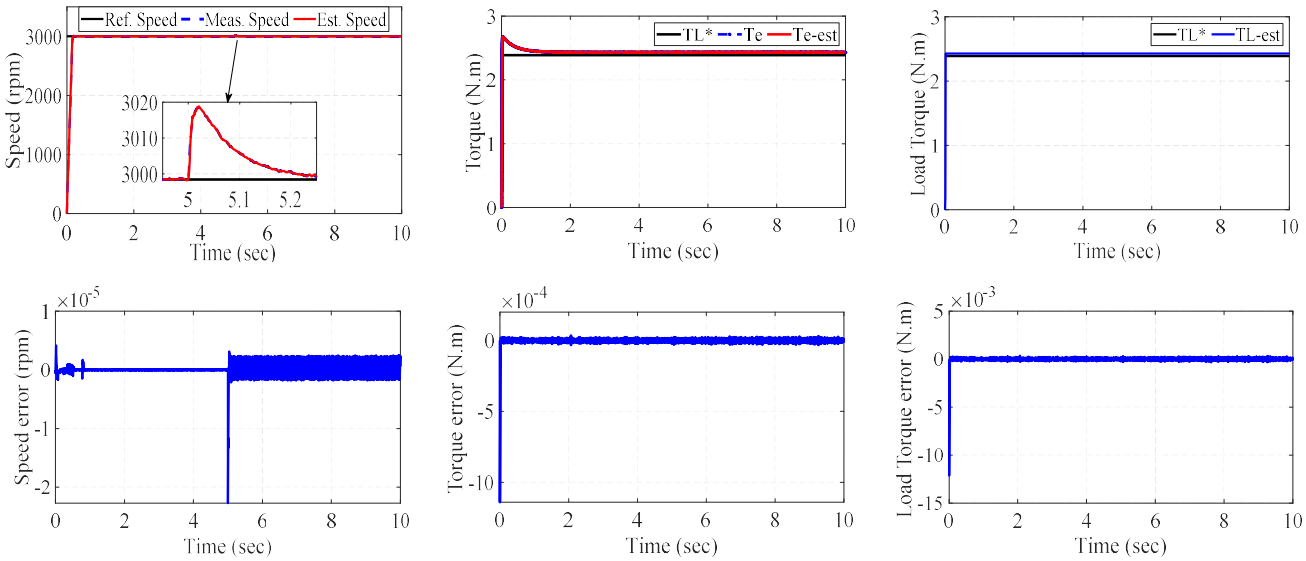

Fig. 7. The 5-phase PMa-SynRM performance using the proposed RTSE, ST-SMSC, and ST-SMCCs at moment of inertia variation condition.

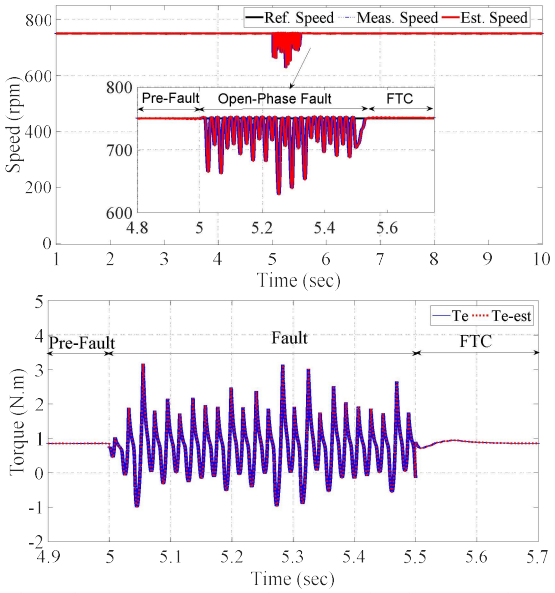

Fig. 8. The 5-phase PMa-SynRM performance using the proposed RTSE, ST-SMSC, and ST-SMCCs under single-phase open fault condition.

The corresponding speed and torque waveforms of the 5-phase PMa-SynRM under pre-fault, open-phase fault, and using FTC are depicted in Fig. 8. As depicted in Fig. 8, the proposed RTSE with the ST-SMSC, and ST-SMCCs proved their robustness alongside the single open-phase fault and estimated the rotor speed and the electromagnetic torque perfectly even during the single open-phase fault and the FTC condition. For pre-fault operation at t=0-5 sec, the torque ripple range is ~0.11-2.5%. Moreover, the rotor speed has a good speed regulation range with low speed ripple of ~0.25-1%. Throughout the single open-phase fault condition at t=5-5.5 sec, the torque ripple increases to ~ 4-30%. Through using the FTC at t=5.5-10 sec, the torque ripple minimizes to ~0.12-2.4%.

G. Sensitivity to the Open Fault of Phases A & B Condition

In order to check the robustness of the proposed the RTSE, ST-SMSC, and ST-SMCCs performance, open-phase fault is occurred in two adjacent phases A & B of the 5-phase PMa-SynRM at t=5 sec and the FTC is adopted at t=5.5 sec. The

corresponding speed and torque waveforms of the 5-phase PMa-SynRM under pre-fault, adjacent two-phase open circuit fault, and using FTC are depicted in Fig. 9. As shown in Fig. 9, the proposed RTSE with the ST-SMSC, and ST-SMCCs proved their robustness alongside the adjacent two-phase open circuit fault and estimated the rotor speed and the electromagnetic torque perfectly even during the adjacent two-phase open circuit fault and the FTC condition. For pre-fault operation at t=0-5 sec, the torque ripple range is ~0.11-2.5%. Moreover, the rotor speed has a good speed regulation range with low speed ripple of ~0.25-1%. Throughout the two-phase open circuit fault condition at t=5-5.5 sec, the torque ripple increases to ~ 6-40%. Through using the FTC at t=5.5-10 sec, the torque ripple minimizes to ~0.12-2.4%. It can be noted that the torque ripple of the 5-phase PMa-SynRM is larger when two-phase are disconnected compared with the single-phase disconnection condition. Therefore, the adjacent two-phase open circuit fault has a great influence on the PMa-SynRM, which directly affects the regular motor operation. Moreover, the torque ripple of the 5-phase PMa-SynRM is nearly the same as that before the fault under the FTC. In addition, the torque ripple is minimized, and the PMa-SynRM can continue to operate stably.

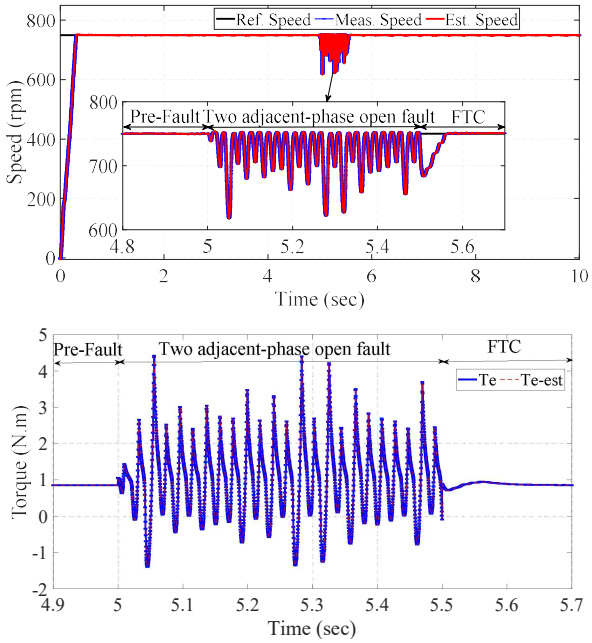

Fig. 9. The 5-phase PMa-SynRM performance using the proposed RTSE, ST-SMSC, and ST-SMCCs under two adjacent-phase open fault condition.

VIII. Conclusion

In this paper, a robust torque-speed estimator has been presented and designed for estimating the rotor speed and the load torque for a 5-phase PMa-SynRM. Moreover, this estimator has solved the speed sensor fault problem, as the feedback speed information was attained directly from the virtual sensor. The stability analysis of the proposed estimator has been achieved via Schur complement along with Lyapunov analysis. Furthermore, for improving the 5-phase PMa-SynRM performance, five super-twisting sliding mode controllers were utilized with providing a robust response without the impacts of high chattering problem.

A super-twisting sliding mode speed controller has been used for controlling the PMa-SynRM rotor speed, and four super-twisting sliding mode current controllers have been used for controlling the 5-phase PMa-SynRM currents. The applicability of the RTSE, ST-SMSC, and the ST-SMCCs approaches have been tested with the 5-phase PMa-SynRM throughout the load disturbance and the electrical and mechanical parameters variations conditions. In addition, as the motor is a multi-phase machine, thus it has been checked against the single open-phase fault and the adjacent two-phase open circuit fault conditions in order to prove the effectiveness of the proposed estimator and the controllers. The experimental validation results proved the effectiveness of the proposed RTSE with ST-SMSC, and the ST-SMCCs approaches due to the superior tracking and the robustness against the electrical and mechanical parameters variations, single open-phase fault and the adjacent two-phase open circuit fault conditions with smaller steady-state errors, robust dynamic behavior, and low torque ripples.

References

[1] W. Huang, W. Hua and Q. Fan, "Performance analysis and comparison of two fault-tolerant model predictive control methods for five-phase PMSM drives," in *CES Transactions on Electrical Machines and Systems*, vol. 5, no. 4, pp. 311-320, Dec. 2021, doi: 10.30941/CESTEMS.2021.00036.

[2] Z. Yin, Y. Sui, P. Zheng, S. Yang, Z. Zheng and J. Huang, "Short-Circuit Fault-Tolerant Control Without Constraint on the D-Axis Armature Magnetomotive Force for Five-Phase PMSM," *IEEE Transactions on Industrial Electronics*, vol. 69, no. 5, pp. 4472-4483, May 2022, doi: 10.1109/TIE.2021.3084172.

[3] M. M. Amin, F. F. M. El-Sousy, O. A. Mohammed, G. A. A. Aziz and K. Gaber, "MRAS-Based Super-Twisting Sliding-Mode Estimator Combined With Block Control and DTC of Six-Phase Induction Motor for Ship Propulsion Application," *IEEE Transactions on Industry Applications*, vol. 57, no. 6, pp. 6646-6658, Nov.-Dec. 2021, doi: 10.1109/TIA.2021.3115088.

[4] M. T. Bin Tarek and S. Choi, "Design and rotor shape modification of a multiphase high speed permanent magnet assisted synchronous reluctance motor for stress reduction," *2017 IEEE Energy Conversion Congress and Exposition (ECCE)*, 2017, pp. 5389-5395, doi: 10.1109/ECCE.2017.8096902.

[5] M. Amin, G. A. A. Aziz, J. Durkin and O. A. Mohammed, "A Hardware-in-the-Loop Realization of Speed Sensorless Control of PMa-SynRM With Steady-State and Transient Performances Enhancement," *IEEE Transactions on Industry Applications*, vol. 55, no. 5, pp. 5331-5342, Sept.-Oct. 2019, doi: 10.1109/TIA.2019.2920960.

[6] N. Bounasla, S. Barkat, E. Benyoussef and K. Tounsi, "Sensorless sliding mode control of a five-phase PMSM using extended Kalman filter," in *Proc. of 2016 8th International Conference on Modelling, Identification and Control (ICMIC)*, 2016, pp. 97-102, doi: 10.1109/ICMIC.2016.7804280.

[7] A. Hezzi, M. N. Abdelkrim and S. B. Elghali, "Sensorless Backstepping Drive for a Five-Phase PMSM based on Unknown Input Observer," in *Proc. of 2020 20th International Conference on Sciences and Techniques of Automatic Control and Computer Engineering (STA)*, 2020, pp. 125-130, doi: 10.1109/STA50679.2020.9329327.

[8] N. K. Nguyen, E. Semail, F. De Belie and X. Kestelyn, "Adaline Neural Networks-based sensorless control of five-phase PMSM drives," in *Proc. of IECON 2016 - 42nd Annual Conference of the IEEE Industrial Electronics Society*, 2016, pp. 5741-5746, doi: 10.1109/IECON.2016.7793553.

[9] B. Tian, M. Molinas, Q. An, B. Zhou and J. Wei, "Freewheeling Current-Based Sensorless Field-Oriented Control of Five-Phase Permanent Magnet Synchronous Motors Under Insulated Gate Bipolar

Transistor Failures of a Single Phase," *IEEE Transactions on Industrial Electronics*, vol. 69, no. 1, pp. 213-224, Jan. 2022, doi: 10.1109/TIE.2021.3053891.

[10] H. Sira-Ramírez, J. Linares-Flores, C. García-Rodríguez and M. A. Contreras-Ordaz, "On the Control of the Permanent Magnet Synchronous Motor: An Active Disturbance Rejection Control Approach," *IEEE Transactions on Control Systems Technology*, vol. 22, no. 5, pp. 2056-2063, Sept. 2014, doi: 10.1109/TCST.2014.2298238.

[11] Z. Zhang, X. Zhang, R. Ma, P. Chen and W. Yang, "Unknown Disturbance Compensation Control of PMSM based on Extended State Observer," in *Proc. of IECON 2021 – 47th Annual Conference of the IEEE Industrial Electronics Society*, 2021, pp. 1-6, doi: 10.1109/IECON48115.2021.9589859.

[12] X. Niu, S. Cong, D. Wang and W. Chen, "Anti-Disturbance Dynamic Surface Control for Position Tracking of Interior Permanent Magnet Synchronous Motor Based on Nonlinear Extended State Observer," *IEEE Access*, vol. 9, pp. 84180-84190, 2021, doi: 10.1109/ACCESS.2021.3086506.

[13] S. Xiong and J. Li, "Cascade Model Predictive Current Control for Five-Phase Permanent Magnet Synchronous Motor," in *IEEE Access*, vol. 10, pp. 88812-88820, 2022, doi: 10.1109/ACCESS.2022.3183138.

[14] P. Chen and Y. Luo, "Analytical Fractional-Order PID Controller Design With Bode's Ideal Cutoff Filter for PMSM Speed Servo System," in *IEEE Transactions on Industrial Electronics*, vol. 70, no. 2, pp. 1783-1793, Feb. 2023, doi: 10.1109/TIE.2022.3158009.

[15] Q. Geng et al., "An Improved PWM Method of Five-Leg VSI Fed Dual-PMSM System With Duty Cycles Regulation," in *IEEE/ASME Transactions on Mechatronics*, vol. 27, no. 6, pp. 5771-5779, Dec. 2022, doi: 10.1109/TMECH.2022.3190690.

[16] S. Liu, C. Liu, Z. Song, Z. Dong and Y. Huang, "Candidate Modulation Patterns Solution for Five-Phase PMSM Drive System," in *IEEE Transactions on Transportation Electrification*, vol. 8, no. 1, pp. 1194-1208, March 2022, doi: 10.1109/TTE.2021.3104876.

[17] Z. Kuang, B. Du, S. Cui and C. C. Chan, "Speed Control of Load Torque Feedforward Compensation Based on Linear Active Disturbance Rejection for Five-Phase PMSM," in *IEEE Access*, vol. 7, pp. 159787-159796, 2019, doi: 10.1109/ACCESS.2019.2950368.

Ghada A. Abdel Aziz (Member, IEEE) received the B.Sc. and M.Sc. degrees in electrical power and machines engineering from Minofiya University, Egypt, in 2006 and 2009, respectively, and the Ph.D. degree in electrical power and machines engineering from Cairo University, Egypt, in 2015. Currently, she is an associate professor at Electronics Research Institute (ERI) in Egypt. From 2006 to 2008, she was a TA with several academic institutions in Egypt. Since 2009, she joined the ERI, as a research assistant, where she has been a researcher since 2015. She was awarded as the best researcher at ERI due to her published papers at the IEEE, in 2018 and 2019, respectively. Her current research interests include control of electrical machines, electrical machines drives, fault-tolerant control, fault-tolerant design of the electric machine, and power electronics in renewable energy systems. She has a patent No. 30183, entitled "A method to detect the phase angle and frequency of the utility grid using the virtual power", which has been issued from the Scientific Research Academy in Egypt in February 2021.

Rehan Ali Khan received a Doctoral degree from the College of Electrical Engineering, Zhejiang University Hangzhou, P.R China. He did Master degree in Electronics and Communication from the University of Lahore, Pakistan in 2013 and Bachelor degree in Telecommunication Engineering from Balochistan University of Information Technology, Engineering and Management Sciences Quetta, Pakistan in 2010. He is working as an Assistant Professor at the Department of Electrical Engineering, University of Science & Technology Bannu, Pakistan since 2011. Research interests include Optimization, Computational Electromagnetics, Smart Grids and Wireless Communication.